Near-infrared Spectral Characterization of Solar-type Stars in the Northern Hemisphere

Collin D. Lewin[1] , Ellen S. Howell[2] , Ronald J. Vervack, Jr.[3] , Yanga R. Fernández[4] , Christopher Magri[5] ,
Sean E. Marshall[6] , Jenna L. Crowell[7], and Mary L. Hinkle[4]

[1] Steward Observatory, University of Arizona, 933 North Cherry Avenue, Tucson, AZ 85721, USA; clewin@mit.edu
[2] Lunar and Planetary Laboratory, University of Arizona, 1629 East University Boulevard, Tucson, AZ 85721, USA
[3] Johns Hopkins Applied Physics Laboratory, 11100 Johns Hopkins Road, Laurel, MD 20723, USA
[4] University of Central Florida, 4000 Central Florida Boulevard, Orlando, FL 32816, USA
[5] University of Maine at Farmington, 224 Main Street, Farmington, ME 04938, USA
[6] Arecibo Observatory/UCF, PR-625, Arecibo 00612, PR, USA
[7] NAVWARSYSCOM, San Diego, CA, USA

Abstract

Although solar-analog stars have been studied extensively over the past few decades, most of these studies have focused on visible wavelengths, especially those identifying solar-analog stars to be used as calibration tools for observations. As a result, there is a dearth of well-characterized solar analogs for observations in the near-infrared, a wavelength range important for studying solar system objects. We present 184 stars selected based on solar-like spectral type and $V-J$ and $V-K$ colors whose spectra we have observed in the 0.8–4.2 μm range for calibrating our asteroid observations. Each star has been classified into one of three ranks based on spectral resemblance to vetted solar analogs. Of our set of 184 stars, we report 145 as reliable solar-analog stars, 21 as solar analogs usable after spectral corrections with low-order polynomial fitting, and 18 as unsuitable for use as calibration standards owing to spectral shape, variability, or features at low to medium resolution. We conclude that all but five of our candidates are reliable solar analogs in the longer wavelength range from 2.5 to 4.2 μm. The average colors of the stars classified as reliable or usable solar analogs are $V-J = 1.148$, $V-H = 1.418$, and $V-K = 1.491$, with the entire set being distributed fairly uniformly in R.A. across the sky between $-27°$ and $+67°$ in decl.

Unified Astronomy Thesaurus concepts: Standard stars (1564); Solar analogs (1941)

Supporting material: figure sets, machine-readable tables

1. Introduction

Many observations of solar system objects rely on solar-analog stars in order to analyze the reflected sunlight measured at the telescope. Spectral observations designed to characterize asteroids, in particular, are mostly carried out in visible or near-infrared spectral regions and can provide measurements of size and composition.

Over the past 10 yr, we have been observing near-Earth asteroids using the NASA Infrared Telescope Facility (IRTF) to better understand their surface composition and thermal properties. Near-Earth asteroids near 1 au have significant thermal flux in the 3–5 μm spectral region. With the IRTF/SpeX instrument (Rayner et al. 2003), we measured spectra between 0.8–2.5 and 1.9–4.2 μm using two different modes of the instrument. After the 2014 IRTF upgrade, these wavelength ranges were extended to 0.7–2.5 μm and 1.7–5.3 μm respectively. The combined wavelength coverage encompasses the transition from purely reflected light to a thermally dominated regime. Analysis of the spectra requires careful calibration to separate the effects of viewing geometry, changing heliocentric distance, and rotation of the asteroid from the true variability across the asteroid's surface, which may be present. For this work, we use relative reflectance spectra, defined as the ratio of the asteroid spectrum to that of a solar-type star, normalized appropriately. Although working in absolute flux would have advantages, the significant disadvantage of needing photometric conditions and additional absolute flux calibration would limit our program to too few objects. Instead, we use relative reflectance spectra and model the entire spectral range in a self-consistent way, which has been very successful as

shown in Howell et al. (2018), Magri et al. (2018), and Marshall et al. (2017).

Near-Earth asteroids can appear anywhere in the sky during times of close approach, so we have needed solar-analog stars with a wide sky distribution. On each observing night, we have chosen stars near the asteroid position at the time of observation based on their catalog colors, trying to match those of the Sun. In addition, we also observed at least one well-characterized primary solar-analog star—chosen from the published literature—in order to check the nearby star. On any given night, we compare all the stars to the primary solar analog, and compare each asteroid with each star (further details follow in Section 2). Over the course of this project, we have observed 184 solar-type stars selected based on spectral type and $V-J$ and $V-K$ colors closely resembling those of the Sun. For these observations, stars with $6 < V < 10$ are suitable, with $7 < V < 9$ mag best to reach adequate signal-to-noise at all wavelengths of interest and to prevent saturation in the shorter-wavelength range (low-resolution mode of SpeX).

We aimed to expand our list of well-characterized solar stars as well as produce a catalog of good near-infrared solar-analog stars all over the northern sky. We chose an initial set of eight primary solar analogs for which we have ample observations, with most being included in the lists of solar-analog stars presented in Landolt (1992), Campins et al. (1985), or Hardorp (1980) and the rest being selected for our observations based on their solar-like colors from the Two Micron All-Sky Survey (2MASS), Hipparcos, and Tycho catalogs (Perryman et al. 1997; Høg et al. 2000; Cutri et al. 2003). Using our

classification system (see Section 3.2), we have analyzed the spectra of the 184 stars we have observed, with the goal of reevaluating our initial list of eight primary solar analogs. Here, we present a list of 17 well-characterized, primary solar analogs which we confirm are spectrally consistent over time and lack nonsolar spectral features at low to medium resolution. We also include a table of all 184 stars and their suitability as calibration stars, with spectral plots of all stars in the 0.8–4 μm region.

## 2. Observations and Data Reduction

2.1. Near-infrared Star Observations

As part of our observational program, we measured the spectra of many solar-type stars in order to correct for telluric absorption and the contribution of the solar spectrum in our collected asteroid spectra. All of our near-infrared star spectra were collected using SpeX (Rayner et al. 2003) at the NASA IRTF on 133 nights spanning 2008 May to 2018 October, in both prism (0.8–2.5 μm) and LXD1.9 (2.0–4.2 μm) modes. Spectra collected after 2014 August using post-upgrade SpeX cover an extended wavelength range of 0.7–5.3 μm between both the prism and LXD modes. We used the 0.″8 slit, which was usually comparable to or wider than the seeing at the K band (typically 0.″5–1.″0). In a few cases, we used the 1.″5 slit when the seeing exceeded an arcsecond. The spectral resolution is $\frac{\lambda}{\Delta\lambda} = 200$ in prism mode, and 2500 in LXD mode. The effective spectral resolution with the 0.″8 slit is 0.021 μm, and we sample the spectrum at a uniform 0.015 μm in the prism range. Similarly, in LXD mode the effective resolution is 0.0023 μm and sampled at 0.001 μm. During the observations, we guided using the light reflected from the slit jaws with the 1.0–2.5 μm imaging camera, with an autoguider keeping the object centered in the slit during spectral integrations. We averaged several pairs of observations in each set, typically 4–8 pairs of exposures in each mode, nodded along the slit to collect A and B spectra. Pre-upgrade, we used exposures of 1–10 s in LXD1.9 mode to get good sky subtraction for the calibration stars. Post-upgrade, our exposures are limited to 3 s and two coadds to avoid the sky saturating at wavelengths longer than 4 μm. Internal arc lamps were used for wavelength calibration, along with sky lines at the longer wavelengths. Spectral flat fields were taken with internal lamps, as described in Rayner et al. (2003), at each telescope position, within about 1 hr of R.A. in case of flexure.

2.2. Data Reduction and Atmospheric Correction

A majority of our data reduction, including spectral extraction, consisted of processing our SpeX data with the Spextool software described by Cushing et al. (2004). In both prism and LXD modes, the spatial profile perpendicular to the slit is generated along the profile, and the signal is corrected column by column and extracted along the spectral trace. The spectra are extracted from both nodded slit positions and averaged to make the final spectrum.

We applied Bus's method for correcting telluric water vapor in the prism spectra to fit the telluric contribution by modeling the atmosphere with the known altitude and zenith angle at the time of observation. The details of this method are provided by Rivkin et al. (2004). A similar method was implemented to correct for telluric features in the LXD data and is detailed by Volquardsen et al. (2004). Each star spectrum was matched to a modeled atmosphere with respect to both wavelength and the depth of
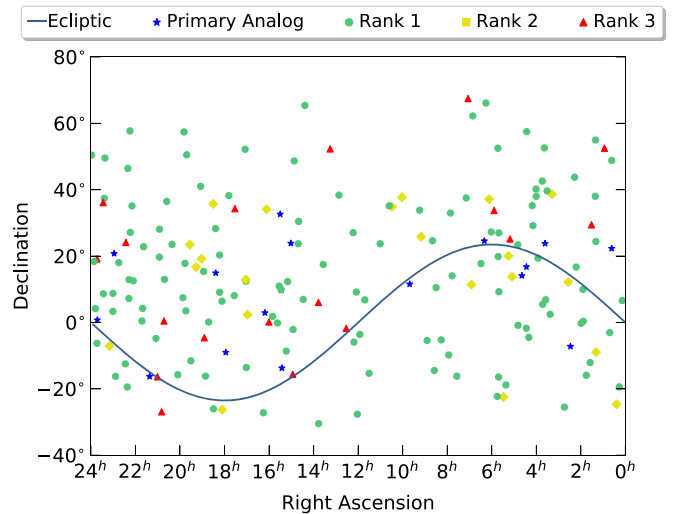
Figure 1. Distribution of our solar-analog candidates across the sky plotted in equatorial coordinates with R.A. in hours and decl. in degrees, with the ecliptic superimposed in blue. Our set of stars spans the sky from $-27°$ to $+67°$ in decl. We have a hole in our distribution from 6 to 12 hr in R.A. and above 40° in decl. for which we have no stars. This hole is further discussed in Section 4. Each of the three rankings assigned to the stars with our classification scheme (see Section 3.2) is plotted in a different color reflecting the results shown in Table 2.

telluric features (Lord 1992). The spread of data points in these features was then iteratively minimized. The best-fit column depth of atmospheric water was determined for the 1.4 and 1.9 μm absorption bands in the prism data, with the average of these two values used to correct for the weaker 0.92 μm water feature. The 3.0 μm absorption band (2.8–3.7 μm) was used to fit the water column depth for the LXD data. Throughout these iterative processes, data points with values outside of 2σ from surrounding points were flagged as bad and ignored in subsequent iterations. Both the prism and LXD spectrum of each candidate star were divided by that of a well-characterized, primary solar-analog star and often several additional candidate stars for our analysis and classification detailed below in Section 3. All data points in the comparison spectra were normalized to unity at 1.65 μm for prism spectra and 2.35 μm for LXD spectra. The $V-J$, $V-H$, and $V-K$ colors—with the J, H, K filter passbands centered at 1.25, 1.65, and 2.20 μm, respectively—of both stars provided by the Hipparcos and 2MASS catalogs were converted from magnitudes to flux units, divided, and plotted with propagated errors in the comparison spectra for comparing the stars' colors. For stars bright enough to have likely saturated in the 2MASS fields, which is indicated by quality codes of C or worse, we utilize colors from VizieR catalog II/225 (Gezari et al. 1999).

3. Candidate Star Classification

3.1. Candidate Selection

When observing many solar system objects, a solar-analog star is utilized to correct or remove the Sun's spectrum from the observed spectrum of reflected sunlight. As a result, such an analog must be readily observed through the same telescopic instrument. In our case of observing near-Earth asteroids, we need stars that are close to the target in the sky on the nights of observation. In the near-infrared, particularly in the 3–5 μm spectral range, the atmosphere changes rapidly on a timescale of minutes. The water vapor content can also change spatially,

Table 1
Final Set of 17 Primary Solar Analogs, with *V* Photometry from the Hipparcos and Tycho Catalogs

Star	SAO Number	Alt. Name	Spectral Type	α(2000)	δ(2000)	*V* (mag)	Nights
HD 3384	SAO 074146		G0	00:36:55.86	+22 18 12.9	8.86 [0.02]	4
BD−07 435	SAO 129922		G0	02:27:58.43	−07 12 12.7	9.74 [0.03]	4
HD 22319	SAO 076021		G0	03:36:28.81	+23 47 50.3	8.62 [0.02]	4
HD 28099	SAO 093936	Hyades 64	G2V	04:26:40.12	+16 44 48.8	8.12 [0.02]	25
HD 29461	SAO 094049	Hyades 106	G5	04:38:57.31	+14 06 20.1	7.95 [0.002]	32
HD 43965	SAO 078236		G0	06:20:05.02	+24 34 00.3	7.64 [0.01]	6
HD 83789	SAO 098710		G0	09:41:11.49	+11 33 25.5	8.79 [0.02]	33
BD+24 2810	SAO 083619		G0	15:01:18.07	+23 51 02.8	9.33 [0.02]	12
HD 137272	SAO 159249		G2/3V	15:25:32.69	−13 44 04.6	9.36 [0.02]	3
HD 137723	SAO 121010		G0	15:27:18.07	+09 42 00.3	7.93 [0.02]	3
HD 138278	SAO 064731		G0	15:29:57.63	+32 37 07.5	8.36 [0.01]	4
HD 145478	SAO 121411		G5V	16:11:06.41	+02 54 51.7	8.66 [0.01]	3
HD 163492	SAO 141976		G3V	17:56:43.12	−09 00 53.3	8.60 [0.01]	3
HD 169359	SAO 103670		G0	18:23:47.06	+14 54 27.8	7.80 [0.01]	9
HD 203311	SAO 164338		G2V	21:21:51.08	−16 16 25.9	7.45 [0.01]	3
HD 217014	SAO 090896	51 Peg	G2IV	22:57:27.98	+20 46 07.8	5.46 [0.05]	14
SA 115−271	⋯		F8	23:42:41.82	+00 45 13.1	9.70 [0.0005]	16

(This table is available in machine-readable form.)

so the best calibration star is located near the target object in the sky so it can be observed frequently through the same atmospheric path.

Near-Earth asteroids can appear in any part of the sky and move rapidly from night to night, motivating a need for a list of solar-type stars spread all over the northern sky and suitable for our observations on the NASA IRTF. Figure 1 shows the distribution across the sky of the stars we have used in our observations, which spans a decl. range of −27° to +67°. For each target on a given night, we search for stars with colors near that of the Sun and within an angular distance of 5° of the asteroid at the time of observation. In a few cases, if no suitable stars are found, the distance is extended to 8°–10°. We also include a primary solar analog to compare the selected calibration star with a known solar-analog star. By "primary solar analog" we mean a star which has been previously determined in the visible to be a good spectral match to the Sun and, after our observations, has been added to our list of primary solar analogs presented in Table 1. To avoid confusion between terminology, a "solar twin" has previously been defined by Cayrel de Strobel (1996) as a star with physical parameters (mass, chemical composition, metallicity, etc.) similar to, if not identical to, the Sun. We use this term in our paper for describing Hyades 106, which we find to be our most reliable primary solar analog. For the purposes of this paper, and for matching the spectral slopes in the near-infrared, primarily 1–2.5 μm, these other character-istics are less important.

We have observed our set of primary solar analogs over many nights, allowing us to confirm their reliability, consis-tency, and lack of nonsolar spectral features, as further discussed in Section 3.3. We selected these stars to calibrate asteroid spectra, which do not usually have narrow spectral features at low to medium resolution. We prefer G0-G5 stars to avoid spectral features, but have found that the stellar spectra are not always as predicted (see Section 4). Stars that showed features were not used as calibrators, so that spurious spectral features were not introduced into the asteroid spectra, and these

stars are labeled "rank 3" according to our classification scheme detailed below in Section 3.2.

Our calibration stars were also selected for having $V-J$ and $V-K$ colors closely resembling those of the Sun, for which we assume solar colors of $V-J = 1.116$, $V-H = 1.426$, and $V-K = 1.486$ (Campins et al. 1985). We prioritize $V-K$ resemblance, typically selecting stars to match $V-J$ within ±0.08 and $V-K$ to within ±0.06. Figure 2 shows the $V-J$, $V-K$ color distribution of our stars. Although a $6 < V < 10$ star is usable for our asteroid spectra calibration, $7 < V < 9$ is preferred for an adequate signal-to-noise ratio in a short period of time at long wavelengths, while still avoiding detector saturation at short wavelengths. The typical uncertainties for both $V-J$ and $V-K$ colors is 0.025 mag, shown on the plot. Individual uncertainties for each star are given in Table 2.

3.2. Classification Scheme

Our classification scheme for assessing a candidate's resemblance to the Sun consists in ranking the star's comparative spectra and using these results to assign a final ranking of the star. The classification system for both the individual spectra and, subsequently, the star itself are the same, with three ranks based on Δ, the magnitude of the deviation of the relative slope from unity:

1. Rank 1: star is a reliable solar analog; no corrections needed ($\Delta < 10\%$ for prism spectra, $\Delta < 20\%$ for LXD spectra).
2. Rank 2: star requires polynomial-fitting corrections to be a usable solar analog ($10\% \leqslant \Delta < 20\%$ for prism spectra).
3. Rank 3: star is effectively nonsolar in that it is not correctable by polynomial fitting owing to variability, nonsolar features, or spectral shape ($\Delta \geqslant 20\%$ for both prism and LXD spectra).

We assess how similar the spectra of two stars are by determining the amount their comparison spectrum deviates from a flat line at 1.0, the result of dividing two identical
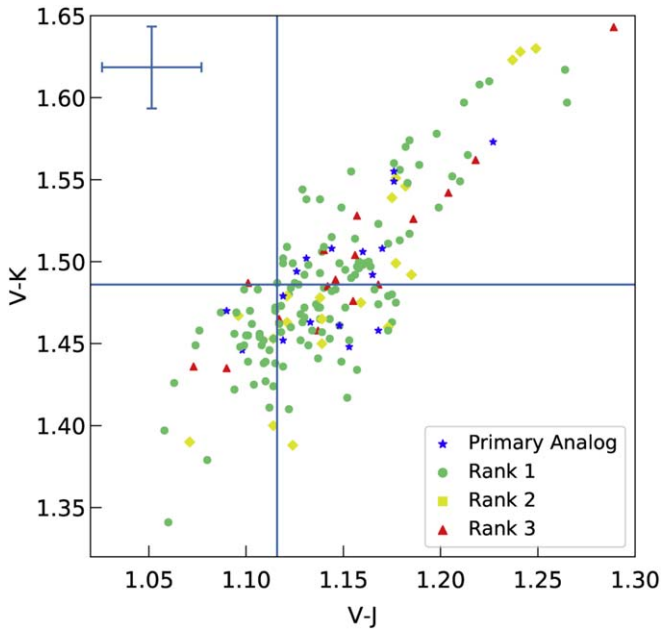
Figure 2. $V-J$ and $V-K$ spectral colors of our set of solar-analog candidates using photometry reported by the 2MASS (for J and K) and either Hipparcos or Tycho catalogs (for V). Assumed solar colors of $V-J = 1.116$ and $V-K = 1.486$ are shown by the blue vertical and horizontal lines, respectively. Each of the three rankings assigned to the stars with our classification scheme (see Section 3.2) is plotted in a different color reflecting the results shown in Table 2. Seven stars (four rank-1 stars, one rank-2 star, and two rank-3 stars) fall outside the axes limits, which are constrained for clarity. The typical uncertainties for both $V-J$ and $V-K$ is 0.025 mag, as shown in the upper-left corner.

spectra. Each comparison spectrum was first fit with a second-order polynomial fit, with the maximum deviation of the fit from a flat line at 1.0 being our statistic for quantifying the deviation from a flat line. The maximum percentage that the polynomial fit of the comparison spectrum deviates from a flat line at 1.0 is denoted above as Δ.

The threshold for determining if a spectrum requires a polynomial-fitting correction to be used is based on whether any slope in the spectrum causes the second-order polynomial fit to fall outside of 10% from a flat line at 1.0 for the comparison prism spectra and 20% for comparison LXD spectra. Prism spectra outside the 10% threshold but within 20% are assigned rank 2 if correctable with a low-order (3–4) polynomial fit or rank 3 if the spectral shape cannot be fit with a low-order polynomial. Stars showing significant variability on any timescale or nonsolar, low-to-medium resolution features are also assigned rank 3. Stars whose prism spectra are within the 10% threshold and LXD spectra within 20% and lack features and variability are ranked 1 and are considered to be reliable solar analogs.

Choosing the threshold for maximum Δ for rank-1 spectra is arbitrary, but the 10% threshold for prism and 20% threshold for LXD are about twice the repeatability of measurements of the spectrum of the same star over several nights. An advantage of spectral observations is that absolute calibration is not needed, and thus usable data can be obtained on nights with cirrus or nonphotometric conditions. However, cirrus does reduce the near-infrared sky stability, and can lead to small spectral slope changes and incomplete correction of telluric features from atmospheric lines being broader and sometimes saturated. The difference in this criterion for maximum

deviation between rank-1 prism ($<10\%$) and LXD ($<20\%$) spectra is a consequence of the relationship between the signal-to-noise of the spectra in these two modes. The asteroid spectra at LXD wavelengths greater than about 3.5 μm is dominated by thermal emission, and so is relatively brighter by a factor of 10–100 than at 2 μm, despite having larger fractional uncertainties.

By our criteria, all but five of our candidate solar-analog stars are rank 1 in the LXD range, so the primary focus of our classifications is on the prism wavelength range. Our final rank for each star is based on the prism spectra. We do not have LXD observations for 12 of our stars and have several stars for which our only LXD observations have too low signal-to-noise, resulting from star faintness and/or observing conditions, to adequately characterize the star at these wavelengths. In this case, we include a note in Table 2 to identify such stars.

Classifications were first assigned to the prism and LXD spectra comparing the candidate star on each observational night to well-characterized, primary solar analogs. If all the comparisons of the candidate star's spectra to primary solar analogs are ranked 1, the candidate is assigned rank 1. However, if several of these spectra are rank 2, we classify the star using the average Δ calculated from those for the individual comparative spectra. Examples of a rank 1, rank 2, and rank 3 prism spectrum are provided in Figure 3 for clarity; the complete set of comparison prism spectra is available as an online figure set sorted by R.A. The rank 1 spectrum (top) is almost entirely flat, with the entire polynomial fit falling within 10% from a flat line. The rank 2 spectrum (middle) has a clear positive slope, resulting in the left end of the polynomial fit falling just outside of 10% but within 20% from a flat line at 1.0. Although the bottom spectrum falls within the 20% levels, there are distinct spectral features from 1.0 to 1.6 μm resulting in a spectral shape that deviates significantly from the polynomial fit; thus, we classify it as rank 3. A similar example for a rank 1 and rank 3 LXD spectrum (we remind the reader that there is no rank 2 for LXD spectra) is shown in Figure 4. The rank 1 spectrum (top) is flat, with the second-order polynomial fit falling within 20%. The rank 3 spectrum (bottom) clearly exhibits prominent features centered at 2.95 and 3.5 μm. The complete set of comparison LXD spectra is available as an online figure set sorted by R.A.

3.3. Set of Primary Solar Analogs

In order to assess the viability of each candidate star as a solar analog, we must first construct a set of reliable solar analogs to use in the evaluations. To that end, we assembled an initial set of eight primary solar analogs, with the majority chosen from the lists of solar-analog stars presented by Landolt (1992), Campins et al. (1985), or Hardorp (1980) and the remaining stars being selected for their solar-like colors from the 2MASS, Hipparcos, and Tycho catalogs. We have ample observations of this set of eight stars, with the number of observations ranging from 6 to 33 nights and an average of 17 nights for the entire set.

To determine whether or not our initial primary analogs are truly viable as solar analogs, we carried out two tests. First, we divided each primary analog's spectra by the spectra of the other seven to ensure that the stars resemble one another, as solar analogs should, and that they lack nonsolar features. Second, for a given star, we compared spectra from all the

Table 2
Rankings for Solar-analog Candidates Sorted by R.A., with *V* Photometry from the Hipparcos and Tycho Catalogs (Except for HD 217014, Which Is from Vizier Catalog II/225), and *JHK* Photometry from 2MASS

Star	SAO Number	Spectral Type	α(2000)	δ(2000)	V	V–J	V–H	V–K	Errors V	V–J	V–H	V–K	Ranking	Notes
HD 377	SAO 109027	G2V	00:08:25.75	+06 37 00.5	7.59	1.168	1.441	1.474	0.010	0.023	0.023	0.023	1	
HD 1204	SAO 147192	G3V	00:16:22.24	−19 23 58.6	8.77	1.100	1.403	1.455	0.010	0.021	0.022	0.023	1	
CD−25 123	SAO 166233	G0	00:23:38.40	−24 38 54.6	10.01	1.177	1.498	1.551	0.020	0.033	0.050	0.030	2	(1)
BD+48 182	SAO 036507	G0	00:36:43.37	+48 49 41.8	8.67	1.179	1.486	1.556	0.010	0.026	0.020	0.022	1	
HD 3384	SAO 074146	G0	00:36:55.86	+22 18 12.9	8.86	1.119	1.364	1.452	0.020	0.028	0.034	0.026	1	
HD 3964	SAO 128909	G5V	00:42:09.78	−03 03 23.0	8.38	1.206	1.492	1.552	0.010	0.026	0.029	0.026	1	
HD 5372	SAO 021850	G5	00:56:17.37	+52 29 28.5	7.52	1.137	1.393	1.458	0.009	0.021	0.020	0.028	3	
HD 7983	SAO 129224	G3V	01:18:59.99	−08 56 22.2	8.90	1.182	1.488	1.546	0.020	0.034	0.041	0.029	2	
HD 7944	SAO 074636	G0	01:19:26.58	+24 24 11.3	8.50	1.118	1.396	1.457	0.010	0.021	0.026	0.023	1	
HD 8004	SAO 022200	G0	01:20:36.94	+54 57 44.5	7.20	1.112	1.332	1.411	0.010	0.026	0.034	0.026	1	
HD 8100	SAO 054620	G0	01:21:03.98	+38 02 03.1	7.87	1.144	1.412	1.515	0.020	0.031	0.048	0.028	1	
HD 9224	SAO 074767	G0V	01:31:19.52	+29 24 47.1	7.31	1.168	1.429	1.486	0.020	0.028	0.029	0.026	3	
HD 9729	SAO 147888	G2V	01:35:01.48	−12 05 06.6	8.62	1.115	1.394	1.470	0.010	0.026	0.029	0.028	1	
HD 10785	SAO 147997	G1/2V	01:45:16.37	−15 53 44.4	8.50	1.140	1.396	1.484	0.020	0.029	0.039	0.030	1	
HD 11532	SAO 110201	G8III/IV	01:53:18.37	+00 22 23.3	9.71	1.131	1.440	1.538	0.020	0.031	0.055	0.034	1	
HD 11616	SAO 110212	G5	01:54:11.98	+09 57 02.3	7.80	1.139	1.372	1.506	0.010	0.021	0.037	0.026	1	
HD 12165	SAO 129608	G2/3V	01:59:27.85	−00 15 10.9	8.85	1.146	1.416	1.483	0.020	0.030	0.043	0.030	1	
HD 13545	SAO 092833	G0	02:12:29.67	+16 42 02.1	8.16	1.152	1.382	1.417	0.010	0.021	0.026	0.028	1	
HD 13931	SAO 037918	G0	02:16:47.38	+43 46 22.8	7.60	1.148	1.366	1.461	0.010	0.022	0.066	0.031	1	
BD−07 435	SAO 129922	G0	02:27:58.43	−07 12 12.7	9.74	1.160	1.427	1.506	0.030	0.038	0.045	0.040	1	
HD 15942	SAO 093004	G0	02:34:03.64	+12 10 51.1	7.49	1.159	1.399	1.475	0.010	0.023	0.021	0.021	2	
HD 17134	SAO 168012	G3V	02:44:14.62	−25 29 43.4	6.96	1.138	1.431	1.493	0.010	0.026	0.034	0.023	1	(2)
HD 20347	SAO 056320	G0	03:17:44.02	+38 38 21.2	7.28	1.139	1.397	1.450	0.020	0.030	0.027	0.028	2	
HD 20939	SAO 111157	G2V	03:22:42.17	+02 28 07.0	8.82	1.107	1.341	1.456	0.020	0.028	0.039	0.027	1	
HD 21630	SAO 056504	G0	03:31:04.08	+39 38 40.9	8.64	1.139	1.391	1.457	0.010	0.021	0.026	0.021	1	
HD 22197	SAO 111270	G0	03:34:42.86	+06 50 35.9	9.65	1.264	1.533	1.617	0.030	0.040	0.038	0.034	1	
HD 22319	SAO 076021	G0	03:36:28.81	+23 47 50.3	8.62	1.153	1.403	1.448	0.020	0.028	0.031	0.035	1	
HD 232816	SAO 024134	F5	03:38:19.40	+52 35 56.7	9.00	1.154	1.438	1.490	0.009	0.022	0.019	0.022	1	
HD 23111	SAO 111366	G0	03:42:37.85	+05 28 42.6	9.15	1.119	1.412	1.502	0.020	0.036	0.043	0.027	1	
HD 23050	SAO 039061	G2V	03:43:47.70	+42 36 12.1	7.47	1.136	1.422	1.474	0.020	0.033	0.028	0.027	1	
HD 285233	SAO 093672	G0	03:55:21.16	+19 22 51.2	8.84	1.132	1.394	1.449	0.016	0.028	0.029	0.033	1	
HD 279209	SAO 056879	G0	04:00:16.12	+37 59 08.3	9.46	1.121	1.431	1.509	0.020	0.027	0.028	0.030	1	
HD 276024	SAO 039243	G0	04:00:29.40	+40 12 09.2	8.61	1.110	1.363	1.439	0.010	0.021	0.045	0.022	1	
HD 26090	SAO 076473	G0V+G5V	04:08:54.35	+29 11 26.2	8.24	1.115	1.384	1.472	0.014	0.028	0.049	0.030	1	
HD 279527	SAO 057048	G0	04:11:04.86	+35 13 33.0	9.22	1.157	1.413	1.497	0.020	0.036	0.045	0.027	1	
HD 27486	SAO 131121	G2V	04:20:11.38	−04 29 35.2	8.99	1.104	1.351	1.425	0.010	0.031	0.052	0.028	1	
HD 27748	SAO 024601	G5	04:25:54.88	+57 29 42.4	8.57	1.173	1.474	1.511	0.010	0.021	0.021	0.028	1	
HD 28099	SAO 093936	G2V	04:26:40.12	+16 44 48.8	8.12	1.227	1.477	1.573	0.020	0.030	0.041	0.029	1	
HD 28192	SAO 131211	G0V	04:26:48.82	−01 43 28.6	8.07	1.109	1.385	1.452	0.010	0.022	0.037	0.026	1	
HD 29461	SAO 094049	G5	04:38:57.31	+14 06 20.1	7.95	1.131	1.425	1.502	0.002	0.037	0.029	0.021	1	
HD 30625	SAO 131516	G3V	04:49:19.29	−00 52 10.6	8.64	1.198	1.511	1.578	0.020	0.029	0.055	0.028	1	
HD 30572	SAO 076777	G0	04:49:48.03	+23 23 44.7	8.51	1.143	1.369	1.453	0.020	0.033	0.034	0.029	1	
HD 32658	SAO 094308	G0	05:05:26.77	+13 48 10.7	9.28	1.124	1.339	1.388	0.020	0.035	0.053	0.030	2	
HD 33366	SAO 077009	G5	05:10:44.54	+25 08 29.4	8.46	1.142	1.429	1.485	0.020	0.027	0.034	0.027	3	(3)
HD 34031	SAO 077054	G0	05:15:11.60	+20 03 21.9	7.72	1.237	1.538	1.623	0.020	0.035	0.076	0.030	2	
BD−18 1066	SAO 150380	G0	05:21:54.85	−18 50 20.9	10.15	1.212	1.522	1.597	0.026	0.032	0.053	0.035	1	
HD 36108	SAO 170461	F9V	05:28:21.03	−22 26 02.1	6.78	1.096	1.370	1.467	0.010	0.028	0.031	0.026	2	
HD 37685	SAO 113028	G0	05:40:46.35	+09 15 55.6	7.94	1.116	1.427	1.487	0.010	0.029	0.033	0.023	1	
HD 246128	SAO 077384	G0	05:40:46.46	+26 59 53.4	9.03	1.101	1.346	1.455	0.020	0.028	0.033	0.047	1	
BD−16 1205	SAO 150701	G0	05:41:35.30	−16 26 04.3	9.03	1.122	1.427	1.480	0.010	0.031	0.039	0.026	1	
HD 246629	SAO 094791	G0	05:42:49.64	+19 50 50.9	9.49	1.177	1.411	1.475	0.030	0.040	0.038	0.037	1	
HD 37693	SAO 025339	G0	05:43:26.85	+52 29 19.6	7.14	1.151	1.433	1.495	0.010	0.021	0.023	0.022	1	

Table 2
(Continued)

Star	SAO Number	Spectral Type	α(2000)	δ(2000)	V	V−J	V−H	V−K	Errors				Ranking	Notes
									V	V−J	V−H	V−K		
HD 38466	SAO 170778	G1V	05:45:09.11	−22 15 45.8	9.32	1.094	1.373	1.456	0.020	0.034	0.068	0.034	1	
HD 248712	SAO 058544	G0	05:53:39.77	+33 44 15.1	8.81	1.090	1.332	1.435	0.020	0.035	0.039	0.030	3	(4)
HD 250285	SAO 077845	G0	06:01:18.25	+27 16 52.8	9.12	1.110	1.377	1.427	0.020	0.030	0.035	0.031	1	
HD 41478	SAO 058755	G0	06:07:10.00	+37 09 51.4	8.60	1.121	1.412	1.479	0.010	0.021	0.021	0.022	2	
BD+66 436	SAO 013769	F2	06:15:45.02	+66 08 07.4	9.03	0.830	0.884	0.993	0.020	0.030	0.064	0.035	1	
HD 43965	SAO 078236	G0	06:20:05.02	+24 34 00.3	7.64	1.133	1.409	1.463	0.010	0.029	0.023	0.031	1	
HD 45580	SAO 095730	G0	06:29:03.70	+17 44 42.8	7.62	1.156	1.415	1.492	0.010	0.028	0.020	0.022	1	
HD 49158	SAO 013980	G0	06:51:10.33	+62 13 46.3	8.67	1.127	1.398	1.486	0.010	0.025	0.022	0.020	1	
HD 50694	SAO 096268	G0	06:54:48.09	+11 25 56.0	8.08	1.121	1.382	1.463	0.010	0.028	0.037	0.028	2	(5)
HD 51708	SAO 014059	G0	07:03:46.17	+67 27 25.2	7.74	1.157	1.448	1.528	0.010	0.029	0.034	0.028	3	
HD 53991	SAO 059815	G0	07:08:51.08	+37 31 30.3	8.60	1.161	1.424	1.499	0.017	0.029	0.026	0.026	1	
HD 60513	SAO 153080	G2V	07:34:13.16	−16 11 16.0	6.72	1.119	1.389	1.499	0.010	0.023	0.052	0.022	1	
HD 62928	SAO 097231	G0	07:46:51.37	+14 03 19.6	8.46	1.163	1.446	1.500	0.010	0.026	0.021	0.020	1	
BD+33 1603	SAO 060387	G0	07:51:13.10	+32 58 47.6	9.13	1.130	1.385	1.492	0.020	0.034	0.043	0.027	1	
HD 64942	SAO 135272	G3/5V	07:55:58.23	−09 47 49.9	8.34	1.095	1.368	1.469	0.010	0.021	0.034	0.025	1	
HD 69270	SAO 135700	G3V	08:16:06.58	−05 14 32.0	9.35	1.108	1.350	1.449	0.020	0.029	0.060	0.029	1	
HD 71848	SAO 097859	G0	08:29:55.73	+10 28 14.8	8.03	1.109	1.373	1.438	0.010	0.022	0.037	0.025	1	
HD 72892	SAO 154423	G5V	08:34:52.59	−14 27 24.1	8.79	1.184	1.467	1.574	0.020	0.029	0.039	0.028	1	
HD 73510	SAO 080324	G5	08:39:37.12	+24 37 13.6	8.89	1.119	1.364	1.436	0.020	0.028	0.026	0.025	1	
HD 76151	SAO 136389	G2V	08:54:17.95	−05 26 04.0	6.00	1.129	1.470	1.544	0.020	0.042	0.028	0.030	1	
BD+26 1904	SAO 080675	G0	09:10:25.85	+25 48 58.6	10.09	1.114	1.358	1.453	0.040	0.044	0.043	0.043	2	
HD 79282	SAO 061342	G5	09:14:14.56	+33 49 00.9	8.28	1.114	1.359	1.453	0.010	0.026	0.048	0.028	1	
HD 83789	SAO 098710	G0	09:41:11.49	+11 33 25.5	8.79	1.176	1.450	1.549	0.020	0.038	0.045	0.035	1	
HD 86811	SAO 061817	F8	10:01:55.85	+37 44 36.1	8.95	0.952	1.156	1.226	0.020	0.029	0.026	0.024	2	
HD 90681	SAO 062060	G0	10:28:51.39	+34 53 08.4	7.82	1.114	1.369	1.400	0.010	0.026	0.039	0.022	2	
HD 91768	SAO 062148	G5	10:36:22.56	+35 07 20.0	8.84	1.158	1.448	1.500	0.009	0.025	0.020	0.023	1	
HD 95311	SAO 081617	G0	11:00:36.82	+23 42 21.9	8.68	1.128	1.419	1.468	0.010	0.028	0.033	0.025	1	
HD 100022	SAO 156720	G2V	11:30:26.09	−15 19 19.7	9.39	1.128	1.369	1.452	0.055	0.059	0.067	0.059	1	
BD+07 2471	SAO 118998	G5	11:41:57.34	+06 48 24.6	9.89	1.124	1.415	1.499	0.040	0.044	0.048	0.047	1	
HD 103549	SAO 138483	G2/3V	11:55:23.69	−03 35 58.1	8.77	1.102	1.368	1.470	0.020	0.034	0.050	0.029	1	
HD 104516	SAO 180396	G0V	12:02:13.46	−27 38 52.4	8.85	1.107	1.350	1.454	0.020	0.030	0.050	0.026	1	
HD 104924	SAO 119208	G0	12:04:53.51	+09 10 20.5	9.41	1.058	1.325	1.397	0.020	0.039	0.057	0.030	1	
HD 105901	SAO 138636	G3/5V	12:11:17.86	−05 55 33.9	8.18	1.123	1.382	1.484	0.020	0.036	0.035	0.030	1	
BD+27 2103	SAO 082194	G0	12:13:30.59	+27 02 36.5	9.90	1.199	1.469	1.533	0.020	0.028	0.031	0.027	1	
HD 109098	SAO 138836	G3/5V	12:32:04.45	−01 46 20.5	7.31	1.140	1.384	1.507	0.010	0.031	0.034	0.018	3	
BD+39 2571	SAO 063224	G5	12:51:40.44	+38 22 06.8	10.3	1.220	1.558	1.608	0.020	0.045	0.034	0.029	1	
HD 115269	SAO 028691	G0	13:15:19.20	+52 16 40.3	9.05	1.156	1.433	1.504	0.009	0.025	0.034	0.022	3	
HD 118034	SAO 100622	G0	13:33:57.66	+17 28 05.0	8.89	1.134	1.375	1.458	0.010	0.022	0.028	0.021	1	
HD 119856	SAO 204825	G1V	13:46:17.64	−30 28 28.1	8.21	1.130	1.376	1.466	0.010	0.026	0.054	0.028	1	
HD 120050	SAO 120107	G5III	13:46:57.91	+06 01 37.7	9.26	1.204	1.481	1.542	0.020	0.033	0.043	0.048	3	(6)
BD+66 844	SAO 016368	G5	14:23:40.91	+65 23 43.8	9.29	1.144	1.418	1.482	0.020	0.029	0.030	0.028	1	
BD+07 2790	SAO 120476	G0	14:27:55.15	+06 57 05.9	9.24	1.087	1.321	1.469	0.020	0.035	0.059	0.030	1	
HD 129171	SAO 064262	G0	14:40:18.39	+30 26 37.8	7.69	1.114	1.371	1.424	0.010	0.022	0.026	0.026	1	
BD+24 2757	SAO 083468	G0	14:41:18.10	+23 43 19.6	9.01	1.138	1.397	1.465	0.019	0.031	0.038	0.030	1	
HD 131526	SAO 045252	G0	14:52:20.91	+48 40 14.7	7.64	1.175	1.442	1.480	0.010	0.023	0.023	0.021	1	
HD 131715	SAO 140224	F8V	14:55:16.18	−02 06 50.7	8.95	1.106	1.417	1.483	0.020	0.030	0.047	0.029	1	
HD 131790	SAO 158903	G0V	14:56:02.54	−15 39 23.5	8.00	1.155	1.347	1.476	0.010	0.023	0.028	0.021	3	
BD+24 2810	SAO 083619	G0	15:01:18.07	+23 51 02.8	9.33	1.144	1.462	1.508	0.020	0.044	0.031	0.027	1	
HD 134533	SAO 101410	G0	15:10:03.01	+12 20 38.7	9.34	1.151	1.408	1.472	0.020	0.029	0.034	0.029	1	
BD−08 3922	SAO 140388	G0	15:13:44.73	−08 37 12.0	9.61	1.265	1.582	1.597	0.105	0.109	0.113	0.109	1	
HD 137272	SAO 159249	G2/3V	15:25:32.69	−13 44 04.6	9.36	1.170	1.447	1.508	0.020	0.039	0.045	0.031	1	
HD 137723	SAO 121010	G0	15:27:18.07	+09 42 00.3	7.93	1.098	1.325	1.446	0.020	0.027	0.043	0.028	1	

Table 2
(Continued)

Star	SAO Number	Spectral Type	α(2000)	δ(2000)	V	V−J	V−H	V−K	Errors V	V−J	V−H	V−K	Ranking	Notes
HD 137775	SAO 101565	G0	15:27:35.07	+09 53 14.6	8.99	1.097	1.379	1.448	0.020	0.031	0.030	0.030	1	
HD 138278	SAO 064731	G0	15:29:57.63	+32 37 07.5	8.36	1.168	1.392	1.458	0.010	0.021	0.019	0.019	1	
HD 138573	SAO 101603	G5IV−V	15:32:43.65	+10 58 05.9	7.21	1.183	1.468	1.548	0.010	0.023	0.028	0.020	1	
HD 139287	SAO 121093	G2/3V	15:37:18.15	−00 09 49.7	8.44	1.225	1.488	1.610	0.020	0.030	0.043	0.030	1	
HD 141715	SAO 121216	G3V	15:50:26.06	+01 49 08.3	8.28	1.138	1.430	1.538	0.010	0.025	0.050	0.025	1	
HD 143436	SAO 121307	G3V	16:00:18.84	+00 08 13.2	8.03	1.146	1.381	1.489	0.010	0.021	0.026	0.021	3	(7)
HD 144873	SAO 065083	G5	16:06:40.00	+34 06 10.5	8.54	1.241	1.547	1.628	0.010	0.022	0.022	0.021	2	
HD 145478	SAO 121411	G5V	16:11:06.41	+02 54 51.7	8.66	1.165	1.398	1.492	0.010	0.022	0.031	0.023	1	
HD 146070	SAO 184262	G1V	16:15:19.09	−27 12 36.9	7.54	1.132	1.431	1.498	0.010	0.023	0.022	0.022	1	
HD 153227	SAO 121963	G3/5V	16:58:00.44	+02 20 31.1	9.81	1.071	1.333	1.390	0.030	0.036	0.043	0.036	2	
HD 153631	SAO 160227	G0V	17:01:10.76	−13 34 01.7	7.14	1.176	1.477	1.560	0.020	0.030	0.031	0.029	1	
HD 153994	SAO 102542	G0	17:02:21.38	+12 24 50.3	9.51	1.080	1.323	1.379	0.020	0.030	0.030	0.027	1	
HD 154064	SAO 102550	G5	17:02:42.73	+12 56 32.2	8.33	1.177	1.463	1.499	0.010	0.029	0.023	0.019	2	
HD 234382	SAO 030231	G0	17:04:30.40	+52 09 42.1	8.59	1.130	1.395	1.472	0.010	0.026	0.020	0.020	1	
HD 159222	SAO 066118	G1V	17:32:00.99	+34 16 16.1	6.56	1.218	1.484	1.562	0.020	0.029	0.034	0.026	3	(8)
HD 159333	SAO 122512	G0	17:33:52.82	+08 06 13.6	8.88	2.111	2.428	2.496	0.054	0.060	0.058	0.056	1	
HD 162209	SAO 066346	G0	17:48:13.08	+38 13 57.3	7.77	1.107	1.401	1.455	0.010	0.035	0.019	0.021	1	
HD 163492	SAO 141976	G3V	17:56:43.12	−09 00 53.3	8.60	1.126	1.401	1.494	0.010	0.034	0.058	0.031	1	
HD 165290	SAO 186276	G1V	18:06:17.29	−26 17 02.7	9.04	1.185	1.369	1.492	0.020	0.029	0.035	0.028	2	
HD 165672	SAO 123130	G5	18:06:48.81	+06 24 38.0	7.77	1.143	1.419	1.465	0.010	0.022	0.034	0.026	1	
HD 348088	SAO 085831	G0	18:13:06.93	+20 19 34.3	8.91	1.101	1.398	1.439	0.010	0.026	0.035	0.019	1	
HD 167065	SAO 123264	G0	18:13:18.79	+09 05 49.3	8.02	1.164	1.410	1.497	0.010	0.028	0.028	0.029	1	
HD 169359	SAO 103670	G0	18:23:47.06	+14 54 27.8	7.80	1.148	1.397	1.461	0.010	0.021	0.031	0.020	1	
BD+28 2993	SAO 086008	G0	18:24:11.62	+28 17 25.1	9.17	1.173	1.439	1.479	0.010	0.021	0.020	0.023	1	
HD 170331	SAO 186884	G5V	18:29:52.02	−26 01 31.4	8.81	1.168	1.403	1.523	0.020	0.030	0.029	0.029	1	
BD+35 3269	SAO 067043	G5	18:30:25.63	+35 43 39.1	9.13	1.175	1.463	1.539	0.020	0.028	0.026	0.030	2	
SA 110−361	⋯	N/A	18:42:45.01	+00 08 04.7	12.43	1.214	1.499	1.565	0.002	0.010	0.022	0.043	1	(9)
HD 174466	SAO 161908	G2V	18:51:15.80	−16 09 42.5	8.81	1.661	1.923	1.996	0.034	0.039	0.047	0.039	1	
HD 175179	SAO 142780	G5V	18:54:23.20	−04 36 18.6	9.03	1.101	1.400	1.487	0.020	0.030	0.050	0.034	3	
HD 175702	SAO 104268	G0	18:56:05.80	+15 21 56.4	7.67	1.175	1.407	1.463	0.010	0.021	0.022	0.019	1	
HD 176972	SAO 104383	G5	19:01:53.16	+19 10 11.7	7.88	1.139	1.434	1.465	0.010	0.028	0.025	0.019	2	
HD 177780	SAO 048053	G3V	19:04:16.38	+41 00 11.4	8.37	1.149	1.395	1.439	0.010	0.021	0.029	0.025	1	
HD 231043	SAO 104675	G0	19:16:38.92	+16 40 04.9	9.25	1.173	1.389	1.460	0.020	0.029	0.041	0.033	2	
HD 183542	SAO 162700	G2/3V	19:30:35.74	−11 33 43.9	9.71	1.182	1.478	1.570	0.030	0.036	0.056	0.040	1	
HD 184403	SAO 087353	G0	19:33:26.21	+23 29 51.0	7.81	1.249	1.489	1.630	0.010	0.028	0.083	0.021	2	
HD 186427	SAO 031899	G3V	19:41:51.97	+50 31 03.1	6.20	1.210	1.600	1.549	0.020	0.028	0.028	0.026	1	
HD 186413	SAO 124998	G3V	19:44:04.39	+03 30 27.8	7.99	1.112	1.377	1.446	0.010	0.025	0.028	0.026	1	
HD 186932	SAO 105240	G0	19:46:37.82	+17 48 10.5	8.10	1.173	1.426	1.458	0.010	0.025	0.022	9.995	1	
HD 187876	SAO 032031	G0	19:49:12.18	+57 24 33.6	7.76	1.063	1.340	1.426	0.020	0.036	0.060	0.028	1	
HD 187897	SAO 125154	G5	19:52:09.39	+07 27 36.2	7.13	1.074	1.384	1.449	0.010	0.022	0.023	0.023	1	
HD 190524	SAO 163258	G3V	20:05:48.70	−15 45 22.4	8.44	1.137	1.403	1.472	0.020	0.028	0.035	0.027	1	
HD 346383	SAO 088564	G0	20:21:25.03	+23 31 15.6	8.87	1.153	1.391	1.452	0.020	0.033	0.039	0.029	1	
HD 196361	SAO 070242	G5	20:35:38.59	+36 28 29.7	8.24	1.166	1.431	1.483	0.010	0.023	0.022	0.019	1	
HD 197195	SAO 106391	G5	20:41:53.31	+12 58 49.6	8.24	1.060	1.287	1.341	0.010	0.025	0.035	0.019	1	
BD−00 4074	SAO 126133	F8	20:43:11.96	+00 26 13.1	9.90	1.073	1.321	1.436	0.020	0.027	0.064	0.030	3	(10)
HD 198176	SAO 189737	G2V	20:49:24.55	−26 56 14.7	8.73	1.117	1.450	1.465	0.020	0.028	0.029	0.027	3	
HD 199221	SAO 089278	G2V	20:55:02.41	+28 05 25.8	7.81	1.156	1.437	1.514	0.020	0.033	0.030	0.027	1	
HD 353253	SAO 106663	G0	20:55:30.44	+19 41 11.0	9.21	1.099	1.433	1.483	0.020	0.044	0.050	0.028	1	
HD 199898	SAO 164058	G2V	21:00:27.76	−16 22 08.1	9.94	1.289	1.538	1.643	0.040	0.048	0.070	0.045	3	
HD 200633	SAO 145075	G5V	21:04:44.15	−04 49 44.0	8.34	1.140	1.427	1.509	0.010	0.021	0.033	0.022	1	
HD 203311	SAO 164338	G2V	21:21:51.08	−16 16 25.9	7.45	1.119	1.396	1.479	0.010	0.021	0.039	0.023	1	
BD+22 4443	SAO 089861	G0	21:38:01.02	+22 49 08.5	9.32	1.157	1.389	1.434	0.020	0.028	0.039	0.028	1	

Table 2
(Continued)

Star	SAO Number	Spectral Type	α(2000)	δ(2000)	V	V−J	V−H	V−K	V	V−J	V−H	V−K	Ranking	Notes
									Errors					
BD+03 4598	SAO 126983	G0	21:40:41.80	+04 15 08.5	9.71	1.154	1.498	1.555	0.030	0.036	0.047	0.036	1	
BD−00 4251B	SAO 127005	F8	21:42:27.45	+00 26 20.3	9.14	1.189	1.472	1.559	0.020	0.028	0.047	0.033	1	
HD 209793	SAO 107657	G5	22:05:52.20	+12 32 47.5	8.66	1.123	1.390	1.460	0.010	0.023	0.028	0.021	1	
HD 210388	SAO 072067	G0	22:09:22.50	+35 07 45.3	7.47	1.129	1.388	1.463	0.009	0.023	0.026	0.017	1	
BD+26 4382	SAO 090339	G0	22:13:47.31	+27 07 19.9	9.16	1.179	1.462	1.513	0.020	0.033	0.027	0.028	1	
HD 211320	SAO 034223	G0	22:14:47.86	+57 42 38.7	8.62	1.076	1.369	1.458	0.020	0.044	0.035	0.034	1	
HD 211476	SAO 107794	G2V	22:17:15.14	+12 53 54.6	7.04	1.160	1.455	1.498	0.020	0.027	0.026	0.026	1	
BD+06 4993	SAO 127435	G0	22:17:37.41	+07 13 44.0	9.46	1.117	1.433	1.462	0.030	0.040	0.045	0.045	1	
HD 212029	SAO 051893	G0	22:20:23.87	+46 25 05.8	8.51	1.137	1.427	1.441	0.010	0.038	0.033	0.025	1	
HD 212083	SAO 165023	G3V	22:21:59.97	−19 26 07.5	7.87	1.118	1.387	1.473	0.010	0.021	0.023	0.023	1	
HD 212680	SAO 090497	G0	22:25:41.78	+24 06 01.4	8.95	0.775	0.951	0.956	0.020	0.027	0.028	0.026	3	
HD 212816	SAO 165090	G3/5V	22:27:14.89	−12 28 33.1	9.48	1.094	1.336	1.422	0.016	0.024	0.041	0.026	1	
HD 215428	SAO 108146	G0	22:44:53.41	+18 01 43.8	8.50	1.122	1.336	1.410	0.010	0.034	0.022	0.022	1	
HD 216505	SAO 165360	F7V	22:53:38.72	−16 14 28.9	8.94	0.963	1.204	1.237	0.020	0.028	0.039	0.031	1	
HD 217014	SAO 090896	G2IV	22:57:27.98	+20 46 07.8	5.46	1.090	1.230	1.470	0.050	0.054	0.054	0.054	1	(11)
HD 217443	SAO 127890	G0	23:00:37.13	+08 45 01.6	8.08	1.149	1.429	1.533	0.010	0.026	0.039	0.028	1	
HD 217458	SAO 127897	F8/G0V	23:00:46.03	+03 20 37.3	8.59	1.103	1.385	1.462	0.020	0.031	0.037	0.034	1	
HD 218647	SAO 146539	G1/2V	23:09:48.98	−07 05 24.3	8.65	1.138	1.436	1.478	0.020	0.030	0.027	0.029	2	
HD 220284	SAO 052943	G5	23:22:08.80	+49 32 01.6	7.90	1.184	1.443	1.517	0.010	0.022	0.021	0.019	1	
HD 220500	SAO 073225	G0	23:23:54.23	+37 24 20.7	8.48	1.138	1.370	1.472	0.010	0.029	0.050	0.019	1	
HD 220773	SAO 128181	G0	23:26:27.44	+08 38 37.8	7.10	1.099	1.388	1.449	0.010	0.022	0.034	0.020	1	
HD 220845	SAO 073257	G5	23:26:49.69	+36 06 13.7	8.41	1.186	1.451	1.526	0.010	0.025	0.028	0.021	3	
SA 115−271	⋯	F8	23:42:41.82	+00 45 13.1	9.69	1.176	1.434	1.555	0.001	0.020	0.044	0.021	1	
HD 222788	SAO 108793	F3V	23:43:34.70	+19 07 47.4	9.08	0.809	0.985	1.029	0.020	0.031	0.034	0.031	3	
HD 222814	SAO 146870	G2V	23:43:50.66	−06 16 24.8	8.52	1.158	1.402	1.496	0.010	0.025	0.033	0.025	1	
HD 223238	SAO 128385	G5V	23:47:52.41	+04 10 31.7	7.69	1.125	1.392	1.487	0.020	0.048	0.066	0.028	1	
BD+17 4993	SAO 108869	G0	23:51:14.65	+18 21 32.3	9.41	1.115	1.404	1.438	0.020	0.028	0.030	0.034	1	
HD 224465	SAO 035934	G4V	23:58:06.82	+50 26 51.6	6.64	1.148	1.407	1.499	0.020	0.028	0.060	0.027	1	

Note. (1) LXD signal-to-noise too low to adequately characterize. (2) Listed as a spectroscopic binary in SIMBAD. (3) Broad features from 1.0 to 1.7 μm. (4) Rank 3 in LXD range, spectral slope from 3 to 4 μm. (5) Nonlinear spectral shape, smooth but indicative of potential time variability that one may want to avoid. (6) Nonrepeatability in spectra–spectral shape changed significantly between 2012 February and 2012 June. Further investigation encouraged. (7) Spectral shape increases significantly ($\approx$15%) toward the blue end of the prism spectrum (near 0.8 μm). (8) Spectral changes from 2012 to 2015 indicate nonrepeatability. (9) Spectral type not listed on SIMBAD. (10) Ample features, many of which are broad and deep. Prism spectrum decreases rapidly toward the blue end (near 0.8 μm). (11) $V-J$, $V-K$ colors from Vizier catalog II/225.

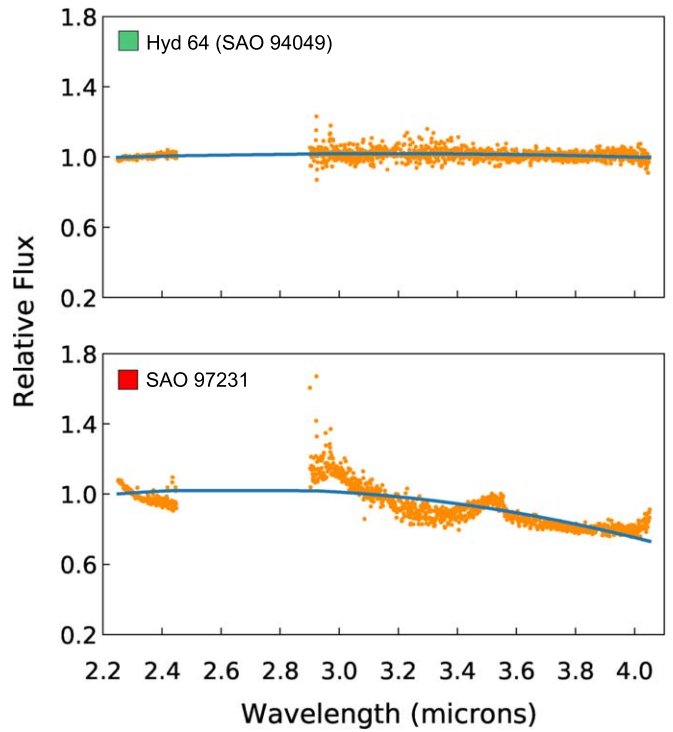(This table is available in machine-readable form.)
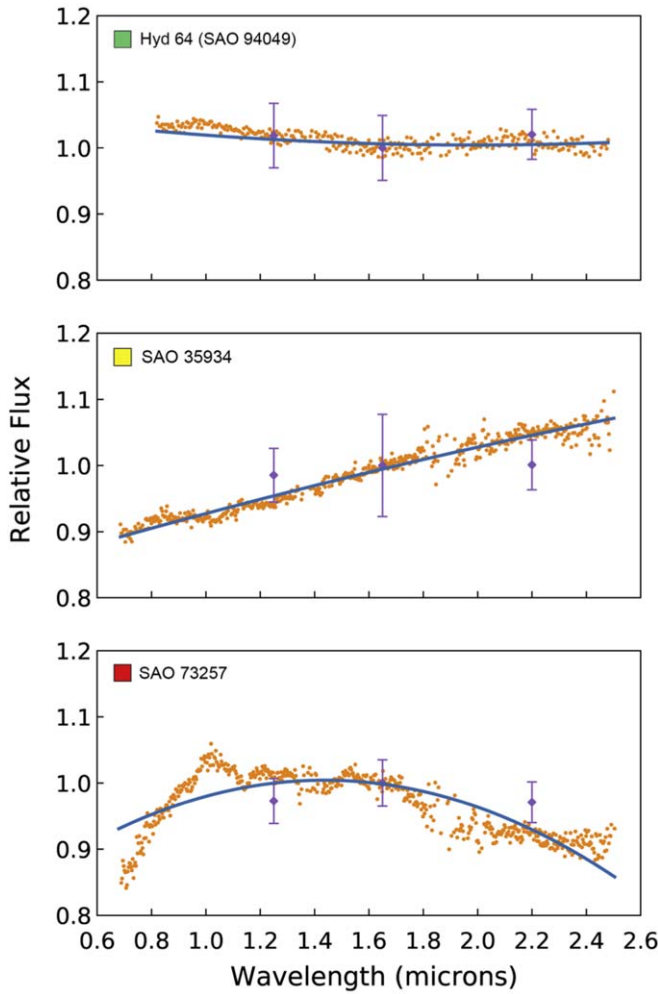
Figure 3. Examples of comparison prism spectra comparing Hyades 64, SAO 35934, and SAO 73257 with a star from our list of primary solar analogs, each with a second-order polynomial fit shown in blue. Relative $V-J$, $V-H$, and $V-K$ colors are plotted with error bars determined from the reported uncertainty in the catalog colors. Each spectrum corresponds to one of the three rankings of our classification scheme outlined in Section 3.2, indicated by the color of the square (top: rank 1, middle: rank 2, bottom: rank 3). Explanations for each of the example classifications are also detailed in Section 3.2. The complete figure set (184 images) is available in the online Journal with stars in order of increasing R.A.

(The complete figure set (184 images) is available.)

Figure 4. Examples of comparison LXD spectra comparing Hyades 64 and SAO 97231 with a star from our list of primary solar analogs, each with a second-order polynomial fit shown in blue. Each spectrum corresponds to one of the two rankings for LXD spectra, indicated by the color of the square (top: green/rank 1, bottom: red/rank 3). The water feature from 2.45 to 2.90 μm has been omitted and is not used in the fitting. The complete figure set (171 images) is available in the online Journal with stars in order of increasing R.A.

(The complete figure set (171 images) is available.)

nights on which it was observed to verify that the star's spectrum is consistent over time.

An example of the first comparison test is shown in Figure 5, where spectra of the seven other initial primary solar analogs have been divided by the spectrum of Hyades 106 (SAO 94049). After determining that Hyades 106 closely resembles Hyades 64 (SAO 93936), a long-known solar analog at visible wavelengths, and is slightly brighter and thus better fit for our asteroid calibrations, we have observed Hyades 106 copiously. Owing to this large number of observations of Hyades 106, we have chosen to designate it as the solar twin in our set (the best solar analog), which we used as the basis for comparison of the other seven stars in our initial set when assessing their reliability as solar analogs.

For each star in the initial set of eight primary solar analogs, a representative spectrum was chosen for the purposes of comparing to the other seven stars. This representative

spectrum was selected as being the most typical spectrum for the star from all the nights on which it was observed. We remind the reader that our process for ranking candidate stars includes a comparison to more than one representative spectrum; instead, we compare all observations of a candidate to those of at least one of our primary solar analogs. We find that all of the spectra comparing each star to Hyades 106 are flat enough to be classified as rank 1 in our classification system (spectrum within ±10% of a flat line), except for the spectrum comparing SAO 65083 to Hyades 106. The red end of the comparative SAO 65083 spectrum deviates by just over 10%, resulting in a rank 2 classification of this star. 51 Peg has been long used as a solar analog in the visible, but its 2MASS catalog colors differ by more than two standard deviations from those of Hyades 106. However, 51 Peg was most likely saturated in the 2MASS fields as shown by the *JHK* quality codes of D, D, and C, respectively. We instead use the pre-2MASS IR photometry presented in VizieR catalog II/225, resulting in 51 Peg's colors being consistent with those of Hyades 106, as shown in Figure 5. We therefore find 51 Peg to be a rank-1 star and, thus, it stays in our list of primary solar analogs.

For the second test of checking for time variability, the representative spectrum for each star was compared to all the other spectra of that star collected throughout our observations. Similar to how we selected a characteristic spectrum of each primary solar analog in our set, the spectra used to compare a star to itself over time were chosen for being representative of
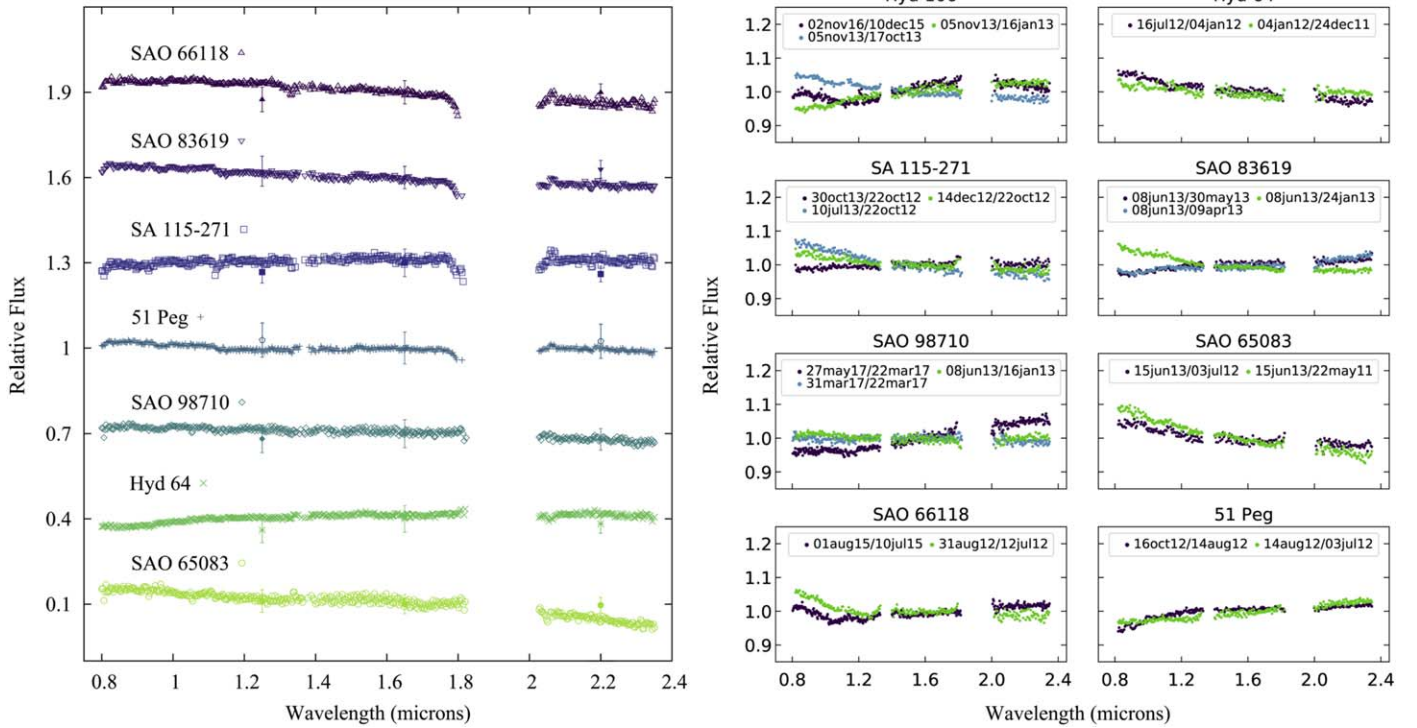
Figure 5. (left) Comparative spectra from dividing each star in our original set of eight primary solar analogs by a representative Hyades 106 spectrum, normalized to unity and shifted for clarity. As described in Section 3, the results of dividing the $V{-}J$, $V{-}H$, and $V{-}K$ colors of each star (in relative flux units) by those of Hyades 106 is plotted with error bars. (right) Comparative spectra from dividing two spectra of the same star collected on different dates. Data leftwards of 0.8 μm has been removed due to instrumental sensitivity drops from 0.7 to 0.8 μm. The telluric water feature centered at 1.9 μm has been removed from all spectra and the 1.35 μm water feature from spectra shown on the right. The results and limitations of these comparisons are discussed in Section 3.3.

the star's other spectra we collected within a month of the observation. As shown in the results of this spectral comparison over time in Figure 5 (right), spectral variations are visible across a timescale of several months in a majority of the solar analogs. However, all of these variations are within $\pm10\%$ from being a straight line, meeting our criterion for assigning a comparison spectrum rank 1; a majority of these changes are within 5%.

Spectra of SAO 66118 showed a distinct change in spectral slope near 1.0 μm in 2015 August that did not appear in 2015 July or earlier in 2012 July. We exclude SAO 66118 from our list of reliable solar-analog stars. We conclude that the remaining stars in the set are reliable calibration stars and are consistent with the solar spectrum at the $<10\%$ level.

Following the above analysis of the initial eight primary solar analogs, we conclude that two of the eight stars in our initial set do not satisfy our criteria for rank 1 solar analogs. Therefore, we have reassessed our original group of primary solar analogs. The stars selected for the list were those that we have both classified as rank 1 and have observed on at least three nights. Most stars selected for the expanded list have also been observed over an extensive timespan, typically between 2 and 5 yr, in order to verify that the star spectrum is repeatable. Our final set of 17 primary solar analogs is presented in Table 1.

When comparing spectra of the same star taken over several years, we found some inconsistencies that appear to be instrumental sensitivity effects. We used five stars with more than 10 separate nights of observation each, and compared them by taking the ratio of each to the overall average spectrum. Figure 6 shows the resulting spectra of four of these,
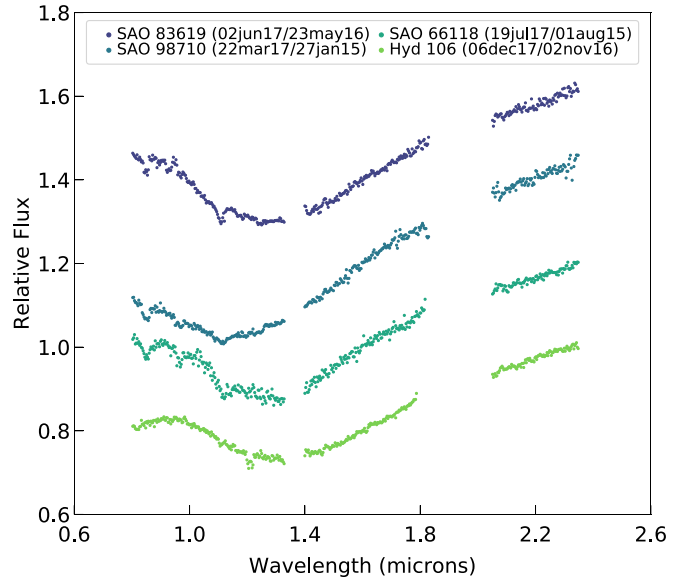
Figure 6. Four examples of the anomalous pattern that often results when comparing two spectra collected more than a year apart following the 2014 IRTF SpeX upgrade. Each spectrum, normalized to unity and shifted for clarity, compares spectra of the same star collected on different nights (listed in brackets). We do not fully understand the cause of this effect but do not think it indicates any change in the stars themselves (see further discussion in Section 3.3).

with an overall pattern of a dip in relative flux between 1 and 1.8 μm. Over shorter time intervals (weeks to a few months) we find that these stars do not show any change in spectral shape. On individual nights the observations of these stars and other
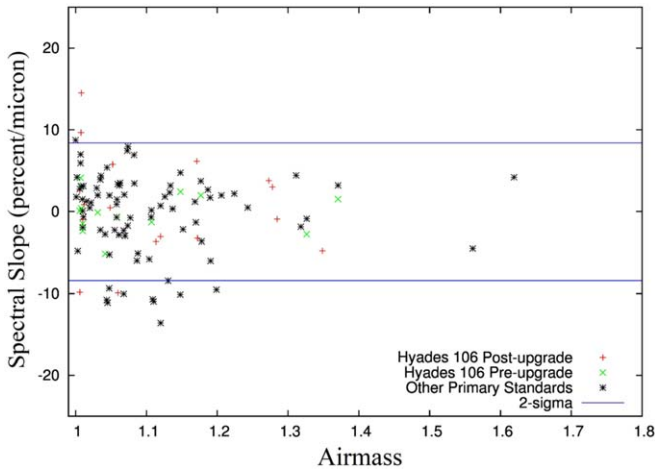
Figure 7. Spectral slopes from 0.85 to 2.45 μm as a function of airmass for observations of Hyades 106 (red and green) and other primary standard stars (black) selected from Table 1. No particular trend arises with observing conditions, though most spectral slope variation occurs at low airmass rather than at high airmass.

solar-analog stars near the asteroid targets are flat to better than the $\pm 10\%$ criterion.

Although we do not fully understand the nature of these spectral changes, it is possible that changes in the telescope instrumental sensitivity, or temporary effects due to weather could be responsible. We are confident that the stars are consistent and that intrinsic variability is not likely to be the cause. We know that there were changes in the telescope and instrument configuration, cleaning of the mirror, changing of the dichroic, and possible ice on the window. However, some specific checks of conditions on particular dates make these seem unlikely. These will not affect the data on a particular night, as they are eliminated by the comparison of the target to the calibration star which both include the same instrument function on a given night.

Our observing procedure does not use the dichroic and we guide directly with the light from the slit jaws. However, some tests indicate that perhaps the centering of the star and short exposures with few coadded images can lead to changes in spectral slope between 0.8 and 1.0 μm, but usually less than our 10% repeatability criterion. We have also checked the influences of airmass on spectral slope and find that there is no particular trend with observing conditions. We have the most spectral slope variation at low airmass, not high airmass. The results of this airmass-spectral slope test are shown in Figure 7.

3.4. Final Ranking of Candidate Stars

We compared the remaining 167 candidate stars by dividing each candidate's prism and LXD spectrum by that of at least one of our 17 primary solar analogs, which is typically observed on the same night of the star. The flatness of the resulting ratio spectrum is indicative of how similar the candidate is to the primary solar-analog star, allowing us to meaningfully compare the two stars. The spectral slopes, features, and relative photometry of the resulting comparative spectrum are then assessed using our classification scheme to assign the spectrum its ranking. Each candidate star is assigned its final ranking on a case-by-case basis by considering the

rankings of the candidate's spectral comparison to one or more of our 17 primary solar analogs.

We present our complete set of 184 solar-type stars, consisting of our final set of 17 primary solar analogs and the remaining 167 candidates, and their assigned rankings in Table 2. Each star's ranking is displayed as a number in the second-to-last column. As delineated in Section 3.2, candidates that are deemed reliable solar analogs without corrections are categorized as rank 1. Stars whose prism spectra need polynomial-fit corrections are rank 2, and those not correctable due to variability, narrowband nonsolar features, or spectral shape are given a rank of 3. Only the star's ranking in the prism wavelength range is presented because we conclude nearly all of our candidates to be rank 1 in the LXD wavelength range. Each star's spectral type, equatorial coordinates (equinox and epoch J2000.0), V (mag), and $V-J$, $V-H$, and $V-K$ colors (in magnitudes) with associated errors are also presented in the table. Any number in the rightmost column corresponds to the footnote describing additional information on a specific star.

4. Discussion

Of our complete set of 184 stars, 145 stars have been classified as reliable solar analogs (rank 1), 21 as needing corrections with polynomial fitting (rank 2), and 18 as not suitable for use as a near-infrared solar standard. The entire set is distributed fairly uniformly in R.A. across the sky, ranging from $-27°$ to $+67°$ in decl. The northern limit is the pointing limit of the IRTF. The overall sky distribution results from the combined effects of our target distribution, weather, and scheduling. Near-Earth asteroids can appear anywhere in the sky when close to Earth. As our program continues, we will fill in more of the sky as needed to find solar-like stars close to our asteroids.

This analysis of the comparison stars also affects the reliability and repeatability of our asteroid spectra. Our choice of the acceptable slope variation for rank 1 stars of 10% is somewhat arbitrary, but is based on our experience estimating our own internal consistency and repeatability. Our choice of $\pm 10\%$ is consistent with the 1σ 4.6% repeatability for SpeX prism observations reported by Marsset et al. (2020), if we assume that 10% is about a 2σ limit, or 95% confidence level. Although we do expect and sometimes see variability in the asteroid spectra, it is generally at a level below 20% in slope, and usually affects only part of the spectrum (most often the 1.5–2.5 μm region). Our observing program is primarily focused on the thermal emission contribution to the spectrum, which for these near-Earth objects is at least 50% of the total flux at wavelengths of 3.5 μm and longer. As we noted earlier, the comparison stars are internally consistent on short timescales of weeks or months. We only see unexplained spectral changes over years, and then mostly at wavelengths shorter than 1.5 μm. Asteroid spectra, particularly S-complex objects, have spectral features in this region that vary by 20% or more from a flat line, due to pyroxene absorptions or other mineral components (e.g., Howell et al. 2018). The additional uncertainty due to the comparison star spectra does not dominate the result. The asteroid targets are always compared to at least two solar-analog stars, often more, and the final spectra are combined using a weighted average. Our targets are usually observed on at least three separate nights over 2–3 weeks, so the consistency can also be checked on different

nights using different nearby stars. Any star that looks like a rank 3 is not included in the analysis. We do not see widespread variability in these measurements but are adjusting our observing techniques to improve the repeatability by doing more coadds for the stars.

4.1. Comparing Our Classifications to Other Literature

Hardorp ([1980](#)) identified four stars—16 Cyg B and Hyades 64, 106, and 142—as the closest solar spectral analogs, often referred to as Hardorp class 1 in the literature, based on their spectral energy distribution in the 3000–8200 Å range in the visible and the ultraviolet line spectra presented by Hardorp ([1978](#)). Of Hardorp's list, our set includes 16 Cyg B (SAO 31899), Hyades 64 (SAO 93936), and Hyades 106 (SAO 94049), for which we have ample near-infrared observations from 0.7 to 5.3 μm. Similar to the classification of Hardorp ([1980](#)), we classify 16 Cyg B, Hyades 64, and Hyades 106 as rank 1, corresponding to reliable solar analogs by our criteria (note we did not observe Hyades 142). We have also included both Hyades 64 and Hyades 106 in our final list of primary solar analogs (see Section [3.3](#)). We observed 16 Cyg B which has been used as a primary standard in near-infrared asteroid studies previously. However, it was often necessary to de-focus the telescope in order to avoid saturation in prism mode. Post-upgrade, although the dynamic range was increased, the minimum exposure time was also increased so that it is impossible to avoid saturation except when the seeing is very bad. We discontinued using this star, although we note that even the de-focused observations have a spectral slope consistent with the overall repeatability of our other standards.

Hardorp ([1980](#)) found the energy distribution of 51 Peg (SAO 90896) to closely resemble that of Hyades 64, which we have classified as a primary solar analog in the near-infrared. 51 Peg has been vetted as a solar analog at visible wavelengths, which we are in agreement with in the near-infrared. We observe the star's spectral shape to closely resemble that of Hyades 106, as shown in Figure [5](#). We were concerned with potential variability from 51 Peg's 2MASS photometry falling outside of two standard deviations from that of Hyades 106, but J, H, and K quality flags indicate that 51 Peg was saturated. Using pre-2MASS infrared photometry from Vizier catalog II/225 resulted in the colors of 51 Peg being in agreement with those of Hyades 106. In addition, 51 Peg has been consistently classified between G2V and G5V throughout the past 70 yr, as shown by Vizier catalog B/mk (Skiff [2014](#)). With 14 observations of 51 Peg, we consequently have classified 51 Peg as both a rank 1 star and one of our primary solar analogs.

After Hardorp ([1978](#)) found its ultraviolet spectrum (3640–4100 Å) to closely resemble that of the Sun, SAO 66118 has been often used as a solar-analog star for observations in both the visible and in the near-infrared. Soubiran & Triaud ([2004](#)) included SAO 66118 in their list of top 10 solar analogs based on the resemblance of both its spectrum in the wavelength range 3850–6800 Å and the star's $B-V$, $U-B$, and $b-y$ colors to those of the Sun. Although we found the near-infrared spectrum of SAO 66118 to roughly match that of solar analog Hyades 106 in our 2012 observation, our 2015 observation shows that the star's spectral shape has changed considerably over the three-year span. The significant change in spectral shape between the 2012 and 2015 observations is shown in Figure [8](#). We classify the star as rank 3 by our classification scheme. Hall et al. ([2007](#)) reported

SAO 66118 to be variable, categorizing the star as a high-activity variable, the class corresponding to the most variable stars of their three classes.

King et al. ([2005](#)) reported SAO 121307 as potentially comparable as a solar analog to HR 6060, once regarded as the closest ever solar twin. This conclusion was based on high-resolution Keck High Resolution Echelle Spectrometer (HIRES) spectroscopic data (4475–6900 Å) in addition to the similarity of the star's effective temperature, luminosity, mass, age, light-metal abundances, and rotational velocity to that of the Sun. Our spectral observations of SAO 121307, however, reveal the spectral shape of the star to increase significantly toward the blue end of the prism spectrum (near 0.8 μm). As shown in Figure [8](#), where the spectrum of SAO 121307 is compared to that of SAO 98710, one of our primary solar analogs, collected on the same night. The blue end of the comparative prism spectrum exceeds the 10% maximum deviation limit from a straight line, but remains within a deviation of 20%. Thus, we classify SAO 121307 as rank 2, or needing polynomial-fit corrections to be used as a solar analog in the prism range of the near-infrared.

Since being used as a Pluto comparison star by Tedesco & Tholen ([1980](#)), SAO 120107 has been used occasionally as a solar-analog star for asteroid spectral observations, primarily in the near-infrared using the IRTF SpeX instrument. The spectrum of the star closely resembles that of many stars in our list of primary solar analogs for all seven of our observations spanning from 2009 June to 2012 February. When we observed SAO 120107 four months later in 2012 June, however, the star's spectral shape had changed significantly and needed to be corrected with polynomial fitting, as shown in Figure [8](#). Although we have ranked SAO 120107 as a rank 3 for variability, the star's spectral shape in our observations is consistently correctable with fitting and thus may be usable for some purposes. We stopped using SAO 120107 as a calibration star after our only anomalous observation in 2012, so further investigation into the star's near-infrared variability may be warranted.

SAO 126133 was included in the set of *UBV* solar-analog stars presented by Landolt ([1973](#)) and has since been frequently utilized as a solar analog in asteroid and comet observations in both the visible and in the near-infrared. When we observed the star in 2008 September (shown in Figure [8](#)), we detected features, many of which are broad and deep, and found the star's spectral flux ratio to decrease rapidly toward the 0.8 μm end. These broad features are centered near 1.6 and 2.3 μm, with the latter being the most prominent. As a result of both the spectral shape and features, we report SAO 126133 as a rank 3 star in our list.

We have concluded that many of the rank 3 stars in our list are not adequate solar analogs for our purposes from 0.7 to 2.5 μm as a result of possessing low-to-medium resolution, nonsolar spectral features in this wavelength range. The set of stars for which we detect such features consists of SAO 126133, SAO 21850, SAO 77009, SAO 14059, SAO 138836, SAO 164058, and SAO 73257. Representative spectra for each of these stars are shown in Figure [8](#). Although such features render the stars unsuitable for our asteroid observations, we believe that these features may be of interest for those studying stellar systems, disks, or planetary systems. Although these stars are not suitable for our calibration purposes, these spectral features or variability may be interesting in themselves for
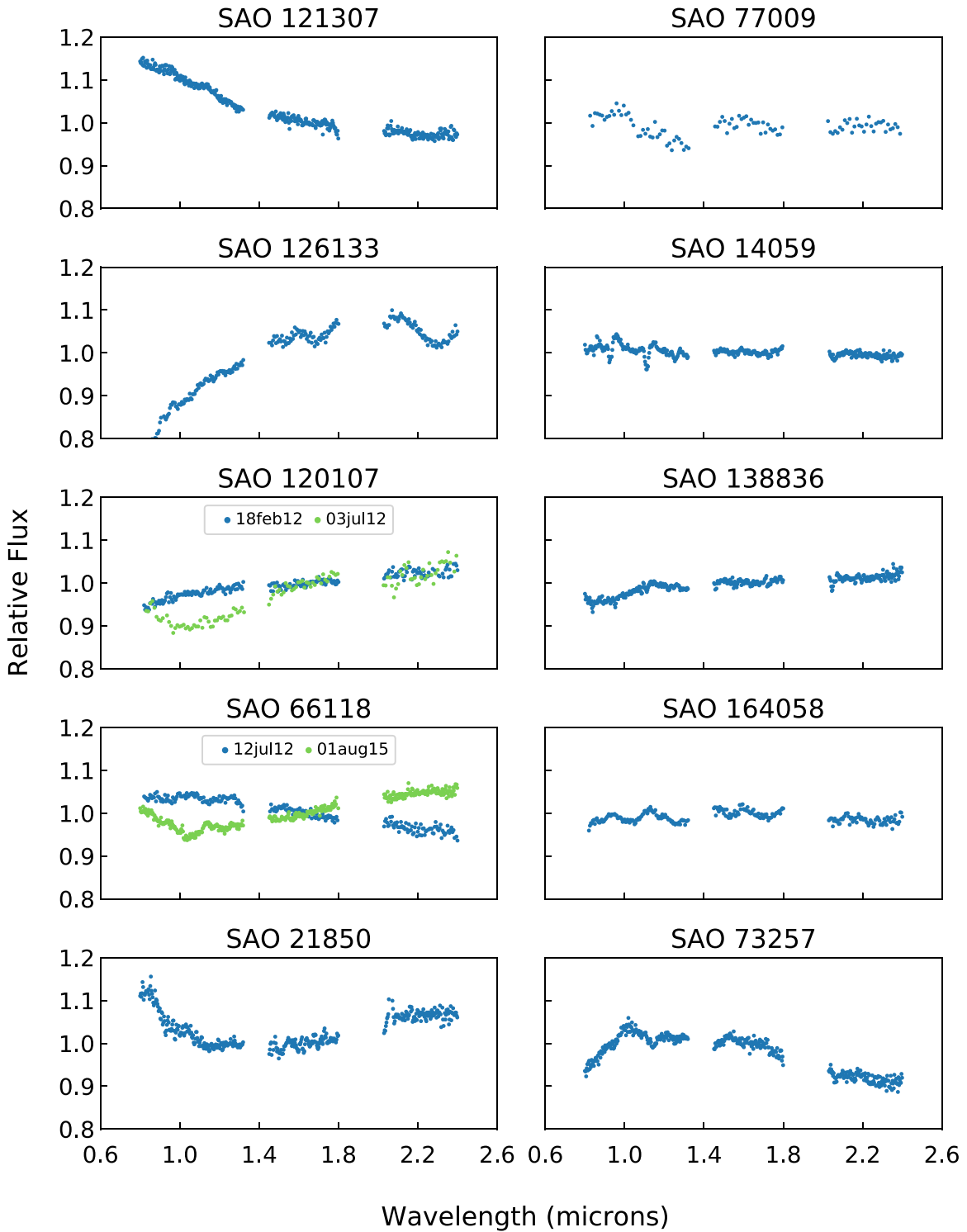
Figure 8. Prism spectra comparing the rank 3 stars discussed in Section 4.1 with one of our 17 solar-analog stars. Stars with only a single spectrum characteristic of the star plotted were assigned rank 3 for having nonsolar features, while those with two spectra plotted show variability on the timescale shown. The telluric water features centered at 1.35 and 1.9 μm have been removed for clarity.

other types of study, so we bring them to the attention of other observers.

5. Conclusion

We have presented a list of 184 stars that we have observed as potential solar analogs as indicated by their catalog spectral type and solar-like $V-J$ and $V-K$ colors, shown in Table 2.

Based on our classification system, each candidate has been assigned one of three ranks indicative of the star's quality as a solar analog from 0.8 to 2.5 μm, shown in the final column of Table 2. Of our set of 184 candidate stars, we conclude 145 to be adequate solar analogs (rank 1), 21 as needing spectral corrections with low-order polynomial fitting (rank 2), and 18 as effectively nonsolar owing to spectral shape, variability, or features at low to medium resolution (rank 3). We conclude

that all but five of our candidates are sufficient, rank 1 solar analogs in the longer wavelength range from 2.5 to 4.2 μm. However, we do not have observations in this wavelength range for 12 stars. The average colors of the stars classified as rank 1 or rank 2 are $V-J = 1.148$, $V-H = 1.418$, and $V-K = 1.491$, with the entire set being distributed nearly uniformly across the sky from $-27°$ to $+67°$ in decl. We present a set of 17 reliable solar analogs we have classified as rank 1 and have observed for more than three nights, prioritizing stars with observations spanning at least 2 yr. We have discovered that several stars studied and vetted as solar analogs at visible wavelengths fail to meet our rank 1 or even rank 2 criteria for solar analogs, most frequently owing to variability or possessing nonsolar features; these stars include SAO 66118, SAO 121307, SAO 120107, and SAO 126133. In addition, we have presented the spectral data of stars in which we observe nonsolar features with the hopes of potentially contributing to research outside the purposes of this paper which may be worth further investigation.

ORCID iDs

Collin D. Lewin ⓘ https://orcid.org/0000-0002-8671-1190
Ellen S. Howell ⓘ https://orcid.org/0000-0002-7683-5843
Ronald J. Vervack, Jr. ⓘ https://orcid.org/0000-0002-8227-9564
Yanga R. Fernández ⓘ https://orcid.org/0000-0003-1156-9721
Christopher Magri ⓘ https://orcid.org/0000-0002-2200-4622
Sean E. Marshall ⓘ https://orcid.org/0000-0002-8144-7570

References

Campins, H., Rieke, G. H., & Lebofsky, M. J. 1985, AJ, 90, 896
Cayrel de Strobel, G. 1996, A&ARv, 7, 243
Cushing, M. C., Vacca, W. D., Rayner, J. T., et al. 2004, PASP, 116, 362
Cutri, R. M., Skrutskie, M. F., van Dyk, S., et al. 2003, yCat, 2246, 0
Gezari, D. Y., Pitts, P. S., & Schmitz, M. 1999, yCat, 2225, 0
Hall, J. C., Lockwood, G. W., & Skiff, B. A. 2007, AJ, 133, 862
Hardorp, J. 1978, A&A, 63, 383
Hardorp, J. 1980, A&A, 91, 221
Høg, E., Fabricius, C., Makarov, V. V., et al. 2000, A&A, 355, L27
Howell, E. S., Magri, C., Vervack, R. J., et al. 2018, Icar, 303, 220
King, J. R., Boesgaard, A. M., & Schuler, S. C. 2005, AJ, 130, 2318
Landolt, A. U. 1973, AJ, 78, 959
Landolt, A. U. 1992, AJ, 104, 340
Lord, S. D. 1992, A New Software Tool for Computing Earth's Atmospheric Transmission of Near- and Far-infrared Radiation, NASA Tech. Memo., 103957
Magri, C., Howell, E. S., Vervack, R. J., et al. 2018, Icar, 303, 203
Marshall, S. E., Howell, E. S., Magri, C., et al. 2017, Icar, 292, 22
Marsset, M., DeMeo, F. E., Binzel, R. P., et al. 2020, ApJS, 247, 73
Perryman, M. A. C., Lindegren, L., Kovalevsky, J., et al. 1997, A&A, 323, L49
Rayner, J. T., Toomey, D. W., Onaka, P. M., et al. 2003, PASP, 115, 362
Rivkin, A. S., Binzel, R. P., Sunshine, J., et al. 2004, Icar, 172, 408
Skiff, B. A. 2014, yCat, 102023, 0
Soubiran, C., & Triaud, A. 2004, A&A, 418, 1089
Tedesco, E. F., & Tholen, D. J. 1980, BAAS, 12, 729
Volquardsen, E. L., Rivkin, A. S., & Bus, S. J. 2004, Icar, 187, 464